

Detection of transient motions with the Global Positioning System

P. Elósegui and J. L. Davis

Harvard-Smithsonian Center for Astrophysics, Cambridge, Massachusetts

J. M. Johansson

Onsala Space Observatory, Chalmers University of Technology, Onsala, Sweden

I. I. Shapiro

Harvard-Smithsonian Center for Astrophysics, Cambridge, Massachusetts

Abstract. To assess the capability of Global Positioning System (GPS) phase measurements for the determination of transient velocity, we have made measurements with a GPS antenna on a moving platform. The antenna was translated in the horizontal plane at a constant velocity of 1 mm h^{-1} for a period of somewhat more than 24 hours while GPS data were recorded simultaneously. Other stationary antennas at distances of 10 m to $\sim 1000 \text{ km}$ were also simultaneously recording GPS data. We calculated an average velocity of the moving antenna by modeling its time-dependent position as a random walk and fitting a straight line to the stochastic estimates. We have found that the accuracy of the resulting velocity estimates is dependent on the observing period and the baseline length. For 24-hour data time spans, rms horizontal velocity errors were less than 0.2 mm h^{-1} for all baseline lengths; for similar time spans, rms vertical velocity errors were $0.3\text{--}0.9 \text{ mm}$ for lengths between 100 and 1000 km, and $\leq 0.2 \text{ mm}$ for baselines $\leq 1000 \text{ m}$. We found it convenient to define a quantity ξ , which we term the dynamic resolution, equal to the ratio of the rms velocity variation to the mean velocity. For a random walk process, ξ_{rw} can be used to calculate the variance per unit time σ_{rw}^2 required by filter-based analysis software. We also investigated the power spectral density (PSD) of our estimates of time-dependent position and found that for the frequency range sampled ($0.07\text{--}16 \text{ mHz}$), the PSD could be well modeled by ν^α , where ν is the frequency and the spectral index α depends on the value of ξ . For strongly constrained (yet unbiased) estimates (obtained by choosing $\xi_{\text{rw}} = 10$ and $\sigma_{\text{rw}} = 0.05 \text{ mm h}^{-1/2}$), the resultant value for α is -4 , indicating a strong filtering of high-frequency noise.

Introduction

The Global Positioning System (GPS) is being used to study geophysical problems occurring on increasingly wide temporal and spatial scales. (See, e.g., *Hofmann-Wellenhof et al.* [1994] and references therein for technical characteristics of GPS and, e.g., *Dixon* [1991] and *Hager et al.* [1991] for reviews of geodetic and geophysical applications.) The vast majority of such studies to date has involved long-term constant rates of (crustal) deformation occurring on regional ($100\text{--}1000 \text{ km}$, say) scales or larger. The method that has typically been employed for the GPS measurements is the so-called “campaign,” which involves discrete occupations of a chosen network of GPS sites, perhaps once or several times per year [e.g., *Davis et al.*, 1989; *Larson*, 1993; *Feigl et al.*, 1993; *Dixon*, 1993]. These studies have furthermore concentrated mainly on the determination of crustal deformation rates associated with plate tectonic motion, which are typically $\geq 10 \text{ mm yr}^{-1}$. Thus, in the main, GPS has been used to resolve length changes in intersite vectors of $\sim 10 \text{ mm}$ occurring over an interval of several

months or more. Each such measurement is taken to be an independent determination of the intersite vector, since it has been assumed (but not demonstrated) that the main sources of error for GPS (satellite orbits, the atmosphere, multipath, and clocks and other instrumentation) do not have long correlation times. Even multipath, which has shown to repeat to some extent from day to day [*Genrich and Bock*, 1992], has not yet been shown to be repeatable over a timescale of months or years.

The issue of the temporal characteristics of GPS errors over timescales of 1 month or shorter has become particularly important because of the advent of continuously operating GPS networks [e.g., *Shimada and Bock*, 1992]. While such networks can obviously be used to study steady state tectonic-driven crustal deformation [e.g., *Shimada and Bock*, 1992; *Larson and Freymuller*, 1995], they can also be used to investigate geophysical phenomena that manifest themselves on much shorter timescales. For instance, GPS was used to measure coseismic displacements of a few millimeters arising from the June 1992 Landers earthquake sequence [*Bock et al.*, 1993; *Blewitt et al.*, 1993]. The temporal characteristics of GPS errors become most important when discussing the detection of motion on the (apparent) “edge” of GPS resolution ability: $\sim 1 \text{ mm}$, whether that motion is occurring over several years or several hours.

Copyright 1996 by the American Geophysical Union.

Paper number 96JB00327.
0148-0227/96/96JB-00327\$09.00

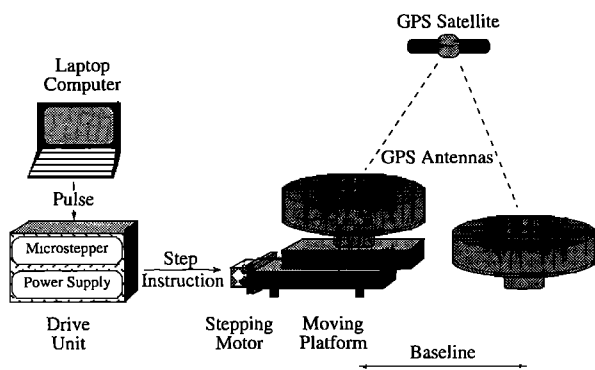


Figure 1. Sketch of the experimental setup. The apparatus consists of a laptop computer, a drive unit, a stepping motor, and a positioning table with a moving platform. A GPS antenna is bolted onto the moving platform. The speed of the platform is software adjustable. See text for details.

Because of the uncertainty in these temporal characteristics, there is no consensus even on the order of magnitude for the accuracy of velocity estimates from GPS for these velocities.

Continuously operating GPS arrays with ground-based receivers spaced tens to hundreds of kilometers will enjoy the unprecedented opportunity to detect transient, short-term (minutes to days) motions, such as the immediate preseismic motions associated with earthquakes, and postseismic motions. Active volcanos may also undergo surface deformation weeks to months prior to eruption. Near-real-time monitoring may be an important component of hazard assessment, earthquake and eruption forecasting, and short-term warning. *Genrich and Bock* [1992] showed submillimeter repeatability using GPS in kinematic mode over a few hundred meter baseline with short (about one-half hour) occupation times. D. M. Tralli (Spectral response of high temporal resolution static Global Positioning System measurements of crustal strain, submitted to *Journal of Geophysical Research*, hereinafter referred to as submitted manuscript) studied the spectral response of GPS measurements for baselines of 10 and 200 km sampled once every 2 min for five consecutive days. He obtained a strain resolution of several parts in 10^6 – 10^7 for the shorter baseline and an order of magnitude better for the longer baseline. *Webb et al.* [1995] obtained 1 mm yr^{-1} precision in the study of the deformation of an active volcanic area from 1 year of continuous GPS observations. *Shen et al.* [1994] measured postseismic deformation with GPS following the Landers earthquake of June 1992. They concentrated on long-term (6-month) deformation, however, and could not resolve the short-term motions directly following the event, since their first data were obtained several days after the earthquake.

In this paper we address the issue of the use of GPS in resolving these small motions over short time spans, 1 day or less. The typical speeds involved are 1 mm h^{-1} . Unlike previous studies, we use an apparatus to move a GPS antenna at just such speeds. We first describe this apparatus and then describe a set of GPS measurements obtained using this apparatus. We present an analysis of the dependence on baseline length and observing time of the velocity resolution. We also discuss the sensitivity of the resolution on parameters representing the temporal resolution of the stochastic filter used to obtain the estimates of position and velocity of the moving antenna.

Experimental Procedure and Data Acquisition

To assess the ability of GPS phase measurements for the determination of velocities, we constructed an apparatus to induce controlled, rectilinear motions on a GPS antenna. Such a system provides an inexpensive, software-independent, flexible method for making this assessment, although in principle, we could achieve the same tests in software only. Field tests with this apparatus were performed in Sweden during 2 weeks in September 1993.

Apparatus

The apparatus (Figure 1) consists of a bidirectional, single-axis positioning table coupled to a digitally controlled stepping motor connected to a laptop computer. The motion of the platform is software adjustable and is ultimately controlled by the number of pulses per unit of time extracted from the computer clock. The direction of motion is established by the orientation of the table.

The controlling computer enables the platform, and consequently, the GPS antenna mounted on top of it, to execute a motion defined by the user: speed, time duration, and direction. A simple program converts the selected speed and time duration into pulse rate and total number of pulses required, and directs the pulses to a Centronics parallel port connected to a stepping motor system. This system consists of a stepping motor and a drive unit, which contains the control electronics (a BiMOS II translator/driver) and a power supply. A standard, permanent-magnet stepping motor geared to 7200 steps per revolution (0.05° step angle) converts the electrical pulses into discrete rotary mechanical motions. A mounting bracket fastens the motor frame to the base of the positioning table, and a flexible coupling transfers the motor shaft motion to a leadscrew, which drives the upper portion of the positioning table. This “carriage” translates smoothly by means of ball-slide rolling elements. The carriage advances 2.54 mm per leadscrew revolution (7200 steps). The GPS antenna is bolted to the carriage by means of mounting holes positioned on top of the table. The dimensions of the slide table are 150 mm (length) \times 75 mm (width) \times 35 mm (height, including the undercarriage).

The instrumental uncertainties for determination of table speed are dominated by the precision of the computer clock. Deviations from the requested path are about $10 \mu\text{m}$ after a movement of 25.4 mm, yielding deviations from the average speed of about $1 \mu\text{m h}^{-1}$ when translating the table at 1 mm h^{-1} for a period of somewhat more than 24 hours. In our tests the table was always driven at a constant rate in the horizontal plane. Excursions from straight-line motion are negligible.

GPS Survey and Data Acquisition

In Figure 2 we show the locations of the GPS sites from which data were acquired. All of the GPS observations used in our analysis were obtained in seven experiments performed between September 3 and 17, 1993 (Table 1), in Sweden, where the SWEPOS network, a permanently operating GPS array [*Davis et al.*, 1993; *Johansson et al.*, 1993], is used to measure three-dimensional crustal deformation rates associated with glacial isostatic adjustment. SWEPOS consists of 20 sites equipped with TurboRogue GPS receivers and Dorne-Margolin antennas with choke-ring groundplane. A choke-ring Dorne-Margolin antenna mounted onto the translation table described above, and connected to a TurboRogue GPS receiver, was placed at the Onsala Space Observatory site.

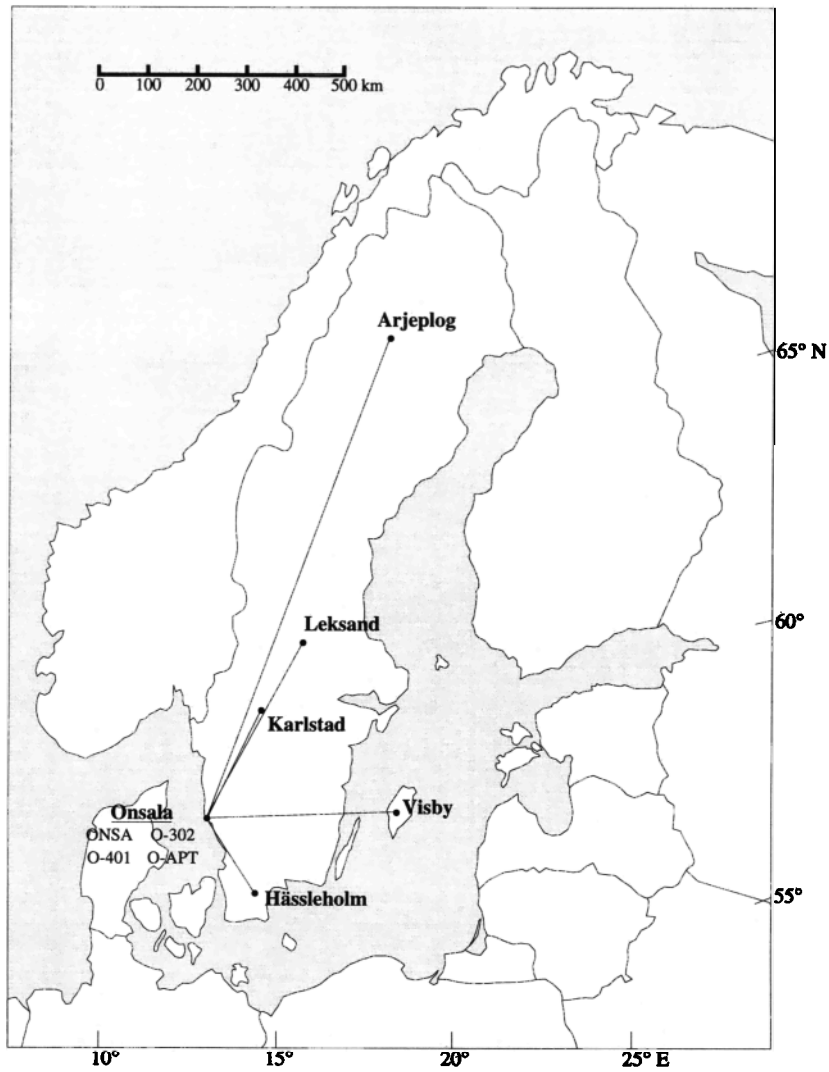


Figure 2. Geographical locations of the sites used in this study. The permanent GPS site ONSA, Sweden, the two translation table sites O-302 and O-APT, and site O-401 are all located within 1 km of each other at Onsala Space Observatory. The other sites shown belong to the Swedish permanent GPS network.

(Brand names are mentioned for identification purposes only.) We chose to make measurements here mainly for logistic reasons.

The ONSA site at the Onsala Space Observatory is part of the International GPS Service for Geodynamics (IGS) network [Boucher *et al.*, 1994]. We occupied two other ground markers with the translation table: O-APT and O-302. The former is a new marker chosen for its presumably almost multipath-free environment. Located on a promontory jutting out into the

Kattegat, the O-APT site has no obstructions above the local horizon. The O-302 site was occupied by the moving platform during four observing sessions and by O-APT during three observing sessions (Table 1).

We acquired GPS data while translating the moving antenna in the horizontal plane at a constant speed of 1 mm h^{-1} for 25.4 hours. For each session the table was kept static for about 2 hours before and after it was set to translate, and on com-

Table 1. Experiments Performed and Sites Used

Starting Day in 1993	Table Location	Fixed GPS Sites						
		Arjeplog	O-IGS	Hässleholm	Karlstad	Leksand	O-401	Visby
Sept. 3	O-302	x	x	x	x		x	x
Sept. 4	O-302	x	x	x	x		x	x
Sept. 5	O-302		x	x	x		x	x
Sept. 8	O-302		x	x	x		x	x
Sept. 13	O-APT		x	x	x	x	x	
Sept. 14	O-APT	x	x	x	x	x	x	x
Sept. 16	O-APT	x	x	x	x	x	x	x

Table 2. Approximate Baseline Distances Between Moving Platform and Fixed Sites

Fixed Site	Distance From O-302, km	Distance From O-APT, km
O-IGS	0.01	1
O-401	0.1	1
Hässleholm	182	182
Karlstad	246	246
Visby	387	387
Leksand	407	407
Arjeplog	1044	1044

pletion of the run, the table was returned to the zero position, from which the next run would start. Each observing session thus lasted a total of ~ 30 hours. The sampling interval used was 30 s. Due to a problem with the storage medium used in the GPS equipment operating at O-302, 10 and 8 hours of GPS data were lost at this site on the third and fourth observing sessions, respectively.

For each observing session, we combined data obtained from the moving antenna and from a maximum of seven stationary antennas (i.e., antennas that remained fixed relative to the crust of the Earth): six TurboRogues from the Swedish network and one additional Rogue at O-401, another marker at Onsala Space Observatory. The receivers operating at ONSA, O-401, and O-302 were connected to the same external 5-MHz hydrogen maser oscillator, although we did not take advantage of this fact when processing the data. The different distances from the stationary sites to the translation table enabled us to sample baseline lengths that ranged from 10 m to 1044 km (Figure 2 and Table 2). (By including the shortest baselines, we do not mean to imply that postseismic motion might be detected on such baselines; instead, these are included for completeness and for understanding the role of baseline length.)

The moving antenna was mounted onto the translation table, which in turn, was bolted onto a ~ 1 m² aluminum plate centered over the respective ground marker by means of a fixed height metallic spike and leveled with four adjustable screws. The same antenna assembly was used at both O-302 and O-APT. The level of the antenna assembly was assured to within $\pm 0.2^\circ$ using a two-axis bubble level mounted on the plate. The antenna assembly was aligned to within $\pm 5^\circ$ of local magnetic north using a hand-held magnetic compass. Antenna heights were measured with an accuracy of ± 0.1 mm by means of a vernier caliper. Antenna leveling, centering, alignment, and height were measured before, during, and after each of the seven sessions, and no differences greater than these quoted errors were ever found. A similar antenna assembly system (without the moving platform) was used for the stationary site O-401. Finally, the axis of the moving platform was oriented, with an accuracy of $\pm 10^\circ$, along fixed local azimuth angles of N210°E (at O-302) and N306°E (at O-APT). These orientations were selected merely to simplify setup at the site. The above orientations of the moving platform result in north and east velocity components, respectively, of -0.87 ± 0.09 and -0.50 ± 0.07 mm h⁻¹ for the first four observing sessions at O-302, and 0.59 ± 0.08 and -0.81 ± 0.09 mm h⁻¹ for the last three at O-APT. (The uncertainties indicated account for errors in drive speed discussed in the previous section as well as

for errors in orientation and leveling.) The vertical speed, for all the sessions at both sites, was 0.00 ± 0.02 mm h⁻¹.

Data Analysis

We used the GPS Inferred Positioning System (GPSY) analysis software developed by the Jet Propulsion Laboratory (JPL) [Webb and Zumberge, 1993, and references therein] for the estimation of the atmospheric zenith delays, clock parameters, phase ambiguities, and three-dimensional, time-dependent relative positions of the GPS antennas. We processed the GPS data independently for each observing session and for each site pair. (Solutions using all eight stations at once would significantly increase the computational requirements and would increase the difficulty in understanding the dependence of the results on baseline length.) The data set for each solution consisted of all the GPS data collected by the two antennas, namely, the carrier-beat phases at the L1 and L2 frequencies and the P-code modulated pseudoranges at the two frequencies [e.g., King *et al.*, 1985], although in practice the pseudorange observables carried little weight relative to the phase observables (factor of 10^2 relative weight). The ionosphere-free phase observables were assumed to have a measurement noise of 10 mm. The phase data were decimated to one sample every 300 s for purely practical reasons: to speed data processing. The satellite orbits were obtained from the JPL daily precise GPS ephemerides [Zumberge *et al.*, 1994], which are determined from a globally distributed network of Rogue GPS receivers. (The data from the ONSA site are included in the JPL solution.) The satellite elevation angle cutoff used was 15° in order to reduce the effects of multipath and atmospheric errors. The a priori propagation delay values used were based on the altitude of the GPS antenna phase center above the geoid plus a nominal value for the wet tropospheric delay of 0.1 m, and were not further adjusted in solutions involving baselines shorter than 1 km. The receiver clock variations were modeled as white noise [Lichten and Border, 1987]. The speed of the translation table, 1 mm h⁻¹, is so small that, for ambiguity-resolution purposes, our experiments can be viewed as static positioning, and hence the integer ambiguity values of the measured phases were successfully determined, and fixed, by applying the Blewitt [1989] carrier-phase ambiguity-resolution algorithm. The estimation of the antenna positions and velocity will be discussed in the next section.

Anti-Spoofing (AS), the deliberate encryption of the P-code signal by the U.S. Department of Defense (DoD), was in effect for the latter part of our (30 hour) observing session beginning September 17, 1993. (When AS is enabled, the non-DoD GPS receivers can no longer acquire the P-code; some of these GPS receivers therefore switch to a cross-correlation mode and acquire the less precise coarse/acquisition code instead.) To process the GPS data for this period, we adopted a slightly different analysis strategy: we deweighted all pseudorange data of AS-affected satellites by an additional factor of 10^3 relative to the weight for the phases (increased from a factor of 10^2 relative weight). Also, we used a minimum elevation angle of 20° instead of 15° .

Determination of Positions and Velocity

A thorough discussion of the different GPS kinematic and dynamic models for the determination of position, velocity, and acceleration along a trajectory has been published by, e.g.,

Schwarz *et al.* [1989], and an account of error sources for kinematic positioning with GPS can be found in the work by, e.g., Lachapelle [1990].

In standard GPS daily processing, the position of each site is typically assumed to remain stationary over the course of the day, and its three components are modeled as constant parameters. In our analysis the dynamic model adopted for the time-dependent position \mathbf{x} of the translation table was a random walk process:

$$\mathbf{x}_{k+1} = S_k \mathbf{x}_k + \mathbf{w}_k \quad (1)$$

where \mathbf{x}_k is the position vector at epoch t_k ; S_k , the state transition matrix at time t_k , is the unit matrix for a random walk process and zero for a white noise process; and \mathbf{w}_k is a vector of normally distributed zero-mean random perturbations. The “true model” for our platform, on the other hand, can be described by

$$\mathbf{x}_{k+1} = \mathbf{x}_k + \mathbf{v} \Delta t_{k+1} \quad (2)$$

where \mathbf{v} is the true constant velocity of the translation table and $\Delta t_{k+1} = t_{k+1} - t_k$ is the interval between two consecutive epochs. Since the Δt_k for our experiments are constant, the parallel between (1) and (2) indicates that using a random walk process to model the position of the moving platform is equivalent to modeling \mathbf{v} as a white noise process, the “least constraining” model for $\mathbf{v}(t)$.

In a rigorous analysis scheme the velocity would appear explicitly in the analysis software as a stochastic parameter. Proceeding in this way, the process noise model would be implemented in the parameter estimation, and the correlations between different parameters would be taken fully into account. For our investigations, we chose not to modify the GIPSY software, which includes a stochastic model for position parameters. Instead, we calculated the velocity of the moving antenna by fitting a straight line to the stochastic estimates of position for the time interval of interest, thus implicitly assuming a rectilinear trajectory for its motion and ignoring the correlations between the estimates of position. (If the velocity were not to remain constant over the course of the observations, one could still try to derive velocities from discrete position measurements using either numerical or digital differentiation. Differentiation will amplify the high-frequency components of the velocity errors and will reduce the low-frequency components [Wei *et al.*, 1991]. Thus, to reduce noise in the high-frequency range, high-accuracy measurements of position and some kind of averaging over a few minutes, or low-pass filtering, may be required.) Figure 3 shows two examples of estimates of the time-dependent position of the translation table, for the same observing session and for two different baselines, for which the velocity is calculated as described above. The time-dependent position estimate from each epoch is treated as an independent unweighted data point.

The variance of the i th component ($i = 1, 2, 3$) of the process noise \mathbf{w} of (1) is

$$\langle w_i(t)^2 \rangle = \langle [x_i(t + \Delta t) - x_i(t)]^2 \rangle = D_i(t, \Delta t) \quad (3)$$

where angle brackets indicate expectation and $D_i(t, \Delta t)$ is the time-domain structure function [Tatarskii, 1961]. For a random walk the structure function is independent of t [e.g., Herring *et al.*, 1990] and is given by

$$D(t, \Delta t) = D(\Delta t) = \sigma_{rw}^2 \Delta t \quad (4)$$

where σ_{rw}^2 is the variance per unit time of the white noise process, which may be thought of as generating the random walk, i.e., a random walk may be expressed as an integrated white noise process. (In (4) and hereafter we omit the subscripts i for simplicity.) The value for σ_{rw} is required as input to the GIPSY software, and it is assumed that all the σ_{rw} components are equal.

Above, we noted that for our particular problem, modeling the position of the moving antenna as a random walk is equivalent to modeling the velocity as a white noise process. From the above paragraph, it is clear that the random walk generating white noise process can therefore be associated with the velocity. In fact, treating the velocity and position as random variables, we have the straightforward relationships

$$\Delta x(t) = x(t + \Delta t) - x(t) = \bar{v}(t) \Delta t \quad (5)$$

and

$$\sigma_{\Delta x}^2 = (\Delta t)^2 \sigma_v^2 \quad (6)$$

where $\bar{v}(t)$ is the average velocity between times t and $t + \Delta t$, σ_v^2 is the variance of velocity, and $\sigma_{\Delta x}^2$ is just the structure function D from (3), which we have explicitly expressed as a variance. Combining (5) and (6), we find the general relationship

$$\frac{\sigma_{\Delta x}}{\Delta x} = \frac{\sigma_v}{\bar{v}} \equiv \xi \quad (7)$$

The parameter ξ is simply an expression of the dynamic variability of a given system with random velocity perturbations. (In (7), Δx and \bar{v} are taken to be positive values; we omit the absolute value symbols for simplicity.) On the other hand, when we use a filter technique, such as is employed by the GIPSY software, then the standard deviations in (7) are input parameters, and so ξ might be viewed as our ability to resolve v or Δx . We will thus refer to ξ as the dynamic resolution parameter. If $\xi \gg 1$, then we will have a weakly constrained solution and will allow for estimated variations in Δx and v which are much greater than the true variations. If $\xi \ll 1$, then we will have a tightly constrained solution.

The dynamic resolution parameter is not the only way to analyze a filter response. For example, for a Kalman filter a more appropriate method of analyzing the response under the assumptions of the filter equations might be to look at the Kalman gain [e.g., Liebelt, 1967]. Such an approach would take into account observational uncertainties (recall we used 10-mm observational uncertainties), as well as the stochastic variances. However, the standard assumptions of the filter equations do not hold in our case, since the velocity, and hence the position increments, are not really random. There is thus no “correct” value for σ_{rw} or for σ_v . The dynamic resolution parameter is thus one measure of the possible bias introduced by using a stochastic filter approach.

In general, if exact information is not available concerning the stochastic process, the weakly constrained solution would be preferable. Herring *et al.* [1990], for example, found that for a range of weak filter constraints the estimated values of the stochastic processes were not significantly affected. The uncertainties of the estimates were significantly affected, however. Too-tight constraints will produce solutions in which the estimates of Δx and v are biased toward zero, whereas weakly constrained solutions allow for greater variation and impose no bias.

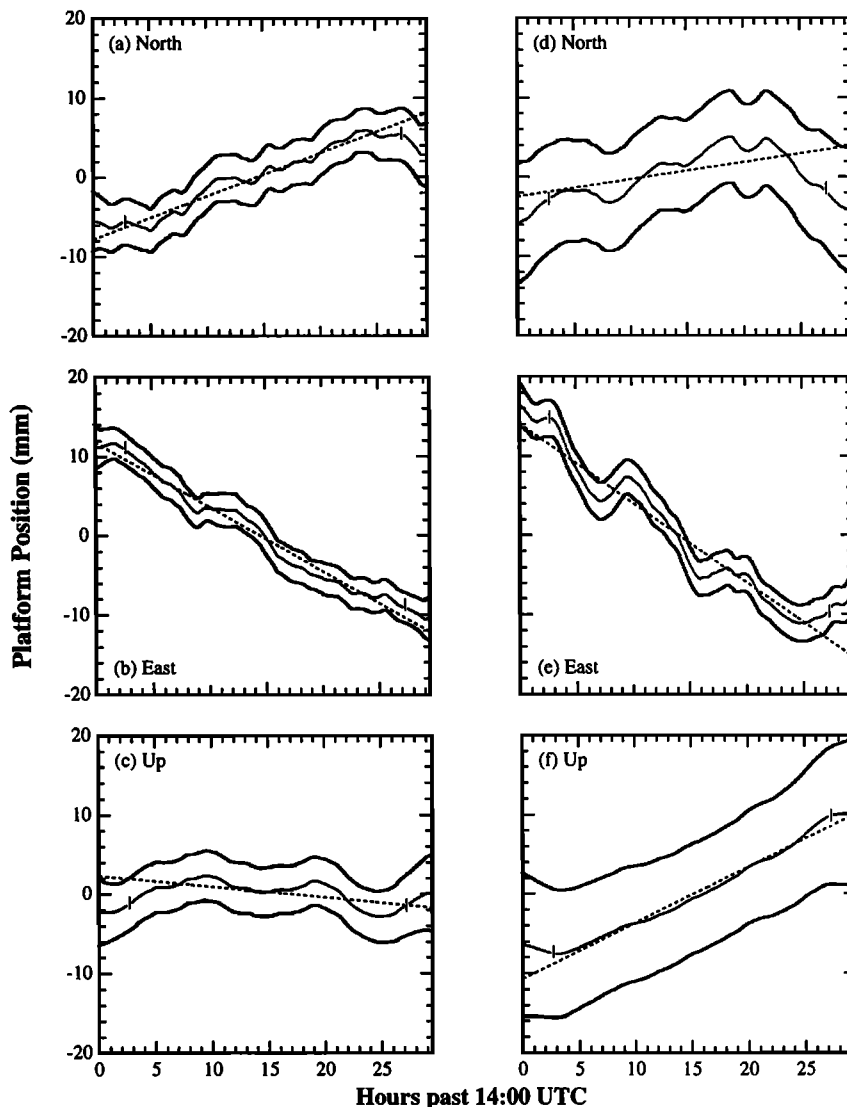


Figure 3. Estimates of the time-dependent position of the moving platform, plotted as a function of UTC hours past 1400 on September 13, 1993, obtained for (a and d) north, (b and e) east, and (c and f) up components for baselines of length (a–c) ~ 0.01 km and (d–f) ~ 1044 km. Each estimate represents a position difference relative to a nominal a priori position. Error “curves” shown are the standard deviations of those estimates, based on the propagated measurement noise of 10 mm. The estimated velocity is computed by fitting a straight line, shown by a dashed line, to the estimated positions for the time during which the antenna was in motion (vertical bars at ~ 3 and ~ 28 hours). The true velocities are (a and d) 0.59 ± 0.08 , (b and e) -0.81 ± 0.09 , and (c and f) 0.00 ± 0.02 , all in mm h^{-1} . The estimated velocities are (a) 0.54, (b) -0.81 , (c) -0.14 , (d) 0.22, (e) -1.00 , and (f) 0.70, all in mm h^{-1} .

One of the advantages in our experiment is that we know our value of $\bar{v}(t)$, which is a constant. Choosing a large value for ξ with respect to unity (say, choosing 10) will thus enable us to calculate a value for σ_v which produces a weakly constrained solution. However, as we mentioned above, the GIPSY software (and other software packages) requires as input σ_{rw} . Using (3)–(7), we can express ξ for a random walk process as

$$\xi_{rw} = \frac{\sigma_{rw}}{v(\Delta t)^{1/2}} = \xi_{rw}(\Delta t) \quad (8)$$

Having chosen a value for ξ_{rw} and an appropriate time interval Δt , and knowing v (or a maximum value for v), we can use (8) to calculate a value for σ_{rw} , the input to the filter software. For our “standard” solutions, which we present below, we chose

$\xi_{rw} = 10$, $v = 1 \text{ mm h}^{-1}$, and $\Delta t = 300$ s, which yielded a value for σ_{rw} of $0.05 \text{ mm s}^{-1/2}$. We chose $\Delta t = 300$ s because in our solutions, we decimated our data to that minimum interval (see above). Below, we discuss the effect of using different values for the parameter σ_{rw} .

Influence of Input Random Walk Variance

We reanalyzed the GPS data using a wide range of values for ξ_{rw} (or, equivalently, σ_{rw} or σ_v) at $\Delta t = 300$ s. The results from this study are summarized in Figure 4. For $\xi_{rw} < 6$ (i.e., $\sigma_{rw} < 0.03 \text{ mm s}^{-1/2}$, or equivalently, $\sigma_v < 6 \text{ mm h}^{-1}$), the estimates of the horizontal velocity tend toward zero, i.e., the filter underestimates the true velocity, which is indicative of a dynamic resolution parameter leading to an overconstrained

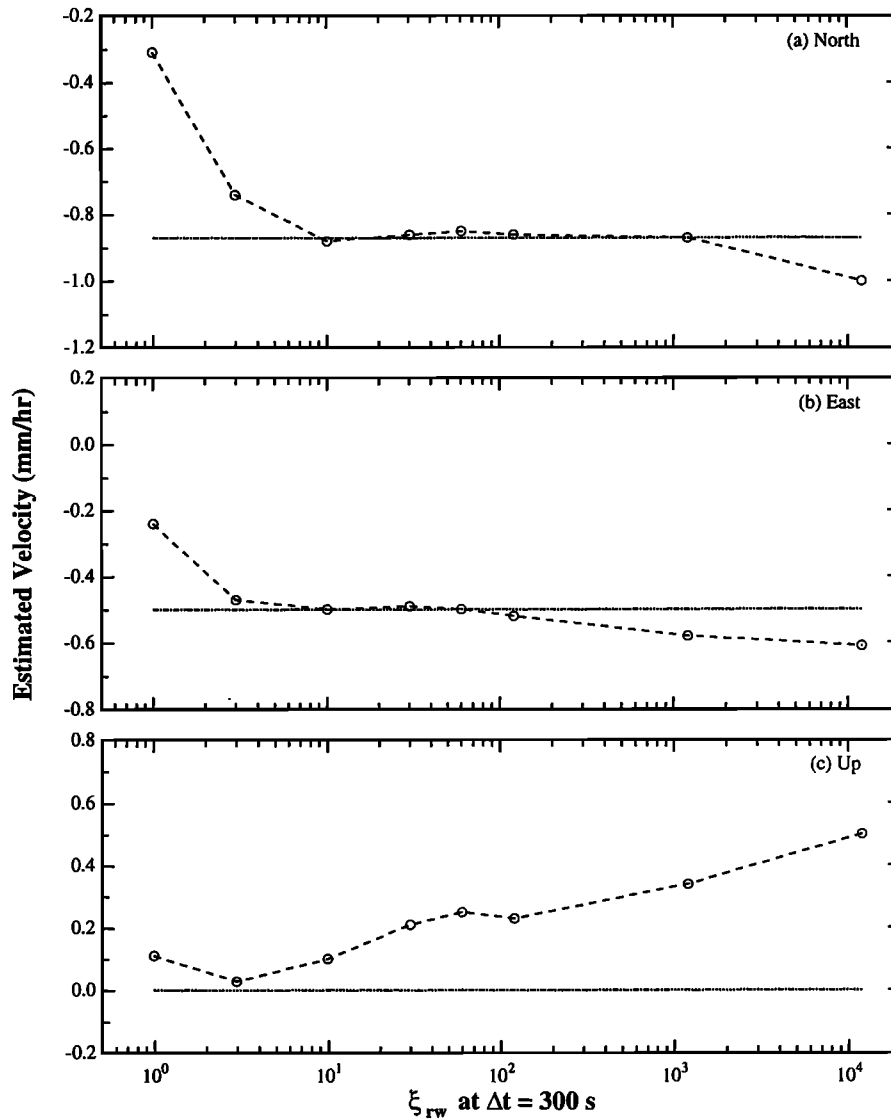


Figure 4. Estimated velocity as a function of the dynamic resolution parameter ξ_{rw} (see text): (a) north, (b) east, and (c) up. The dotted line in each graph represents the true velocity of the translation table.

solution. In fact, this result should not come as a surprise because a random walk process, from (8), has a dynamic resolution parameter which depends on Δt . In our standard solutions the value chosen for ξ_{rw} from (8) was based on a time interval of 300 s, but the estimates of average velocity of the moving antenna were obtained, as explained above, from a linear fit to the stochastic estimates of position from an interval of time of up to 24 hours. From (8), it can be seen that the value of ξ_{rw} for a time interval of 24 hours will be smaller than that for a time interval of 300 s, by an amount equal to the square root of the ratio of 24 hours over 300 s, a factor of approximately 17. For example, for a solution with a random walk variance $\sigma_{rw} = 0.05 \text{ mm s}^{-1/2}$ and an average velocity of $v = 1 \text{ mm h}^{-1}$, a time interval of $\Delta t = 300$ s would yield a value for ξ_{rw} of 10, whereas a time interval of $\Delta t = 24$ hours would yield a value for ξ_{rw} of 0.6. By reversing the argument to determine velocities instead, for a random walk variance $\sigma_{rw} = 0.05 \text{ mm s}^{-1/2}$ and $\xi_{rw} = 10$, the estimates of average velocity would be constrained (at the $1\text{-}\sigma$ level) to $\leq 10 \text{ mm h}^{-1}$ after a

time interval of $\Delta t = 300$ s and to $\leq 0.6 \text{ mm h}^{-1}$ after a time interval of $\Delta t = 24$ hours. The method we chose to determine average velocities from stochastic estimates of the position of the moving antenna thus results in actual constraints that are tighter than if the velocity were estimated explicitly as a stochastic parameter. For the horizontal components, the values $\xi_{rw} < 6$ of Figure 4 correspond to average velocities constrained at the level of 0.4 mm h^{-1} after a time interval of 24 hours; the solution is tightly constrained and the estimates of v are, as expected, biased toward zero. On the other hand, values of $\xi_{rw} \geq 100$ (corresponding to average velocities of 6 mm h^{-1} after 24 hours) do not seem to impose any constraint on the kinematics of the system and also do not describe well the true horizontal motion of the moving platform.

For the vertical component the weakly constrained solutions wander off the true velocity as expected. For the constrained solutions, values of $\xi_{rw} \leq 6$, the estimates for the vertical component of velocity are also in error because estimates of this component, being inherently geometrically “weaker” than

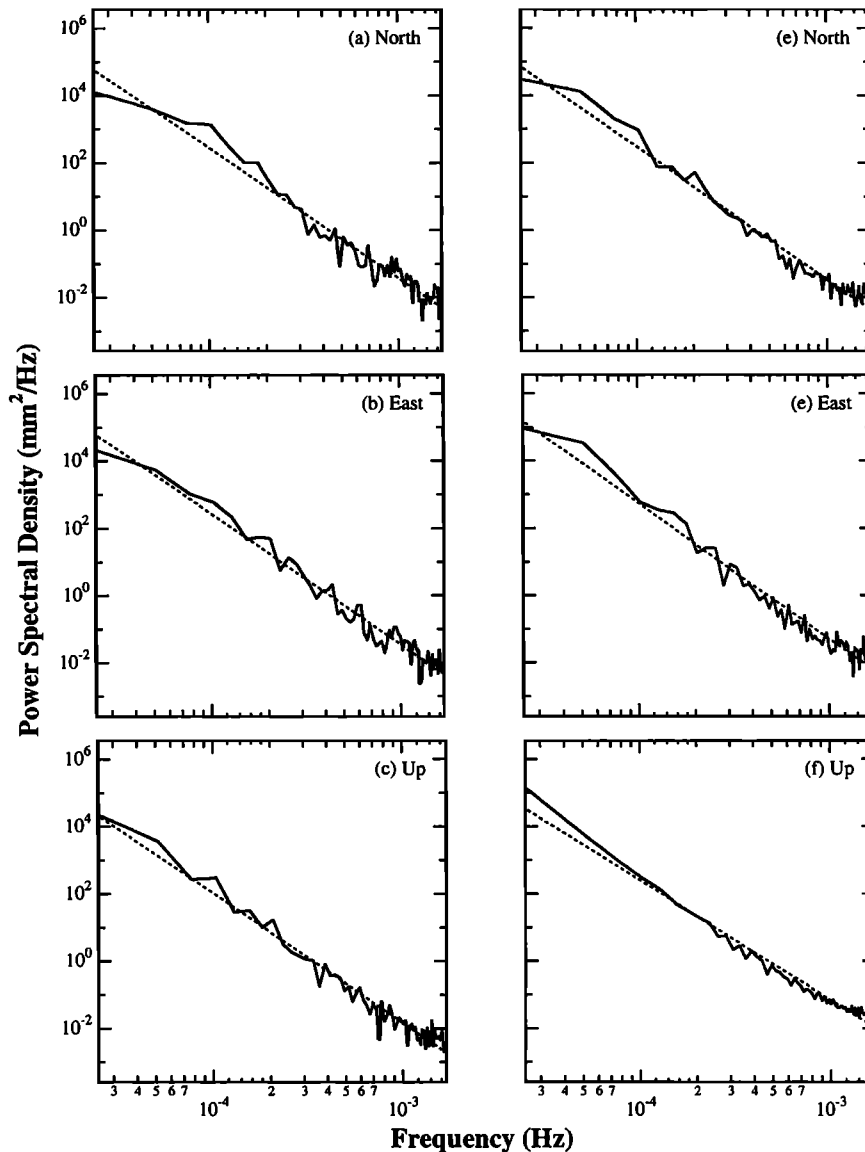


Figure 5. Power spectral density estimates (solid line) of detrended, mean-removed, Welch-windowed time series shown in Figure 3. The estimated spectral indices, i.e., the slopes of the dashed lines, are (a) -3.9 , (b) -3.9 , (c) -3.9 , (d) -4.0 , (e) -4.0 , and (f) -3.6 .

those of the horizontal components, may be affected by the biases in the estimates of velocity observed for the horizontal components.

Determinations of Power Spectra

The time series presented in Figure 3 are dominated by low-frequency variations with typical periods of a few hours. Relatively speaking, high-frequency noise, in the estimates of both the horizontal and vertical components of site position, is nearly nonexistent. The corresponding raw (unfiltered) PSD functions (Figure 5) confirm spectral similarities for all three components. Within the sampled frequency band (0.07 – 16 mHz), the spectrum is inverted, with the power proportional to the sampling frequency raised to a power (spectral index) of about -4 . ($\text{PSD} \propto \nu^\alpha$, where ν is the sampling frequency and α the spectral index; an inverted spectrum corresponds to negative values of α .) These (auto)spectral density functions were determined by first removing an average mean and a

slope from the time series presented in Figure 3, taking overlapping segments from that series, windowing them, and averaging the squared magnitudes of their fast Fourier transforms. Throughout this study the slope removed from the time series was the known true velocity component of the moving platform; the segments were chosen to overlap by one half their length to reduce the spectral variance, each segment consisting of 2^n data points. A Welch window was used to suppress leakage into adjacent frequencies. We experimented with different windowing techniques and found the results to be insensitive to segment length or window function. (For a more detailed description of PSD determination, see, e.g., *Press et al.* [1992] and references therein.) The PSDs of the vertical component have a mean square amplitude larger, by about an order of magnitude, than that of the north component, which in turn, is about a factor of 2 greater than that of the east component. This result agrees approximately with the formal

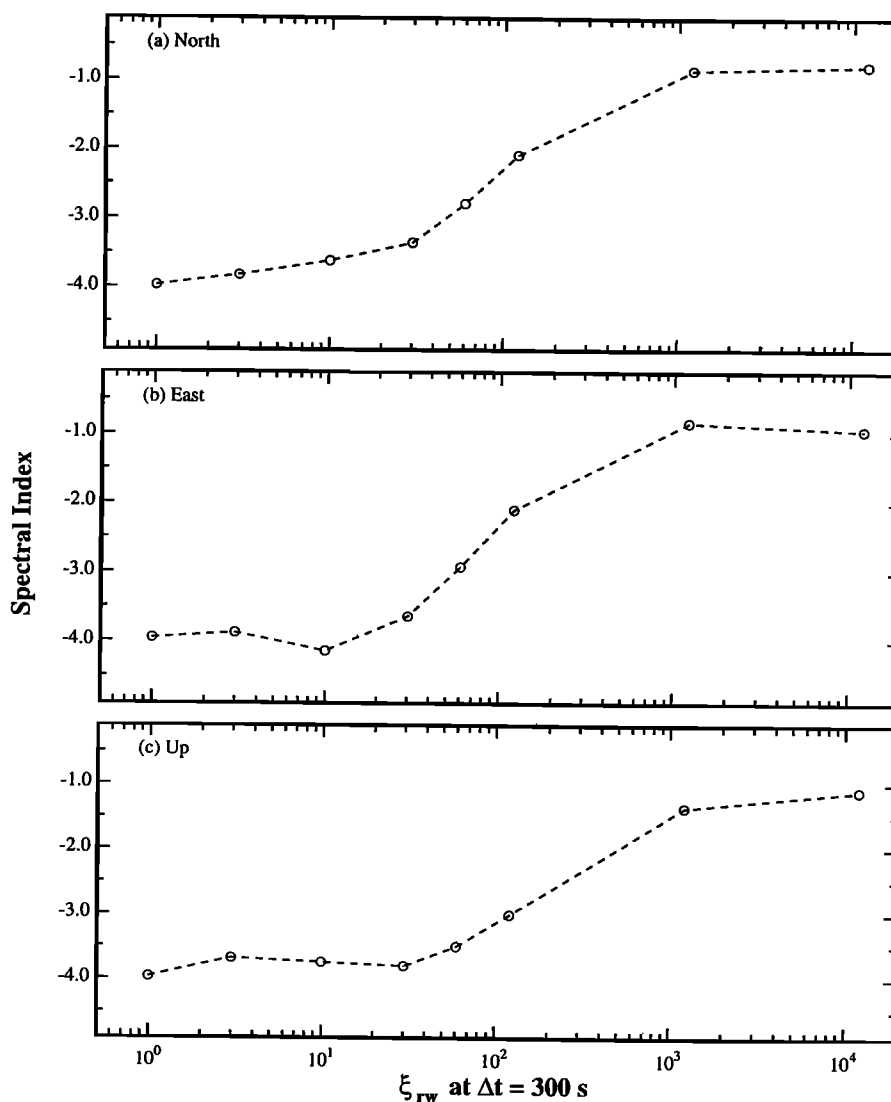


Figure 6. Calculated spectral indices from the power spectral density analysis as a function of the dynamic resolution parameter ξ_{rw} : (a) north, (b) east, and (c) up. A value of -1 is expected for a white noise process.

uncertainties, which reflect the expected better precision for the east component of position than for the north component of position for high-latitude sites, and for better horizontal precision than vertical [e.g., *Santerre*, 1991].

The PSDs obtained are largely independent of baseline length; the spectra presented in Figure 5 for the time series shown in Figure 3 correspond to baselines that differ in length by about 5 orders of magnitude. The spectra are also independent of the specific dynamics of the system; the spectra of two solutions, one involving the moving antenna together with a stationary antenna (see Figure 5), the other involving two stationary antennas, both processed according to the description given above, are similar. None of the spectral indices calculated was found to differ significantly from a value of -4 . We therefore hypothesized that the spectral index of -4 was a measure of the response of the GIPSY filter, rather than a reflection of the noise characteristics of the data. The value of -4 is slightly smaller than we would expect for a random walk process; we calculated a theoretical PSD, based on (4), and obtained a spectral index of -3.3 . Other researchers [*Genrich and Bock*, 1992; D. M. Tralli, submitted manuscript, 1995],

investigating PSDs of GPS determinations of position, have obtained spectral indices closer to -1 or -2 . However, these researchers did not model the positions of the GPS antennas as a random walk.

To test our hypothesis, we investigated the dependence of spectral index on the selection of the value of σ_{rw} used as input to the filter software. The results, shown in Figure 6, indicate that the spectral indices for all three components of site position lie between -4 and -3.5 for $\xi_{rw} \leq 60$ (or $\sigma_v \leq 60$ mm h^{-1}) and rapidly increase (become less negative) as the input variance decreases, i.e., as the stochastic constraint is relaxed, as we would expect. As a further test, we also analyzed one data set in which we modeled the position of the table as a white noise process, instead of as a random walk. In this analysis we allowed for a level of white noise such that the estimates of position were virtually unconstrained. Figure 7 shows the resulting estimates of the time-dependent position of the translation table. A high-frequency noise is now present along with a lower-frequency signal with typical periods of a few hours. The high occurrence of “outliers” in these series, which are caused by a sudden weakening of the satellite geometry,

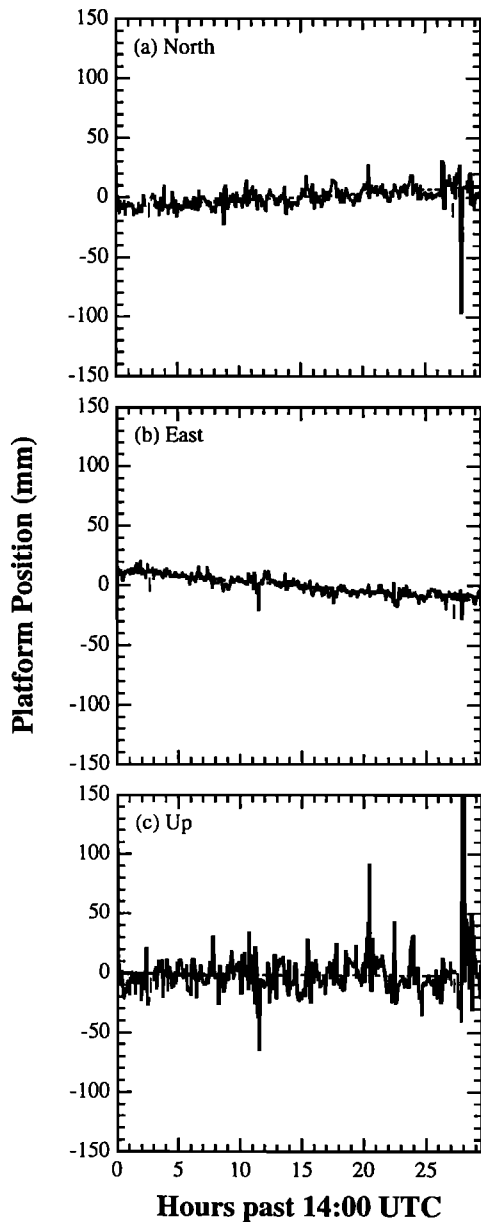


Figure 7. Same as Figures 3a–3c with table position modeled using a white noise stochastic process. The true velocities are (a) 0.59 ± 0.08 , (b) -0.81 ± 0.09 , and (c) 0.00 ± 0.02 , all in mm h^{-1} . The estimated velocities are (a) 0.61, (b) -0.84 , and (c) -0.04 , all in mm h^{-1} . Note the difference in the scale compared to Figure 3.

produces significant errors in the determination of velocity. The corresponding raw power spectra, after average value and slope were removed as explained above, present similar characteristics for all three components (Figure 8), and yield spectral indices of about -1 in the sampled frequency band. Our results for these power spectra, confined to a frequency band $10^{-4} \leq \nu \leq 10^{-2}$ Hz, are consistent with the results presented by *Genrich and Bock* [1992] and D. M. Tralli (submitted manuscript, 1995), who investigated the spectral response of GPS in a frequency band between 1 cycle per day (10^{-5} Hz) and 1 cycle per second (1 Hz) over spatial scales ranging from a few meters to ~ 100 km. These authors attributed the low-frequency part of the spectrum to signal multipath, phase-

center variations, and tropospheric path-delay fluctuations, whereas they attribute the high-frequency part to receiver measurement noise.

Dependence on Baseline Length and Observing Time

We have used the root-mean-square (rms) errors in the GPS estimates of velocity to assess their accuracy, and to determine the dependence of accuracy on baseline length and data time span. The results are summarized in Figure 9. Each point in Figure 9 represents the rms error for a particular baseline, topocentric direction, and time span of data used to obtain the

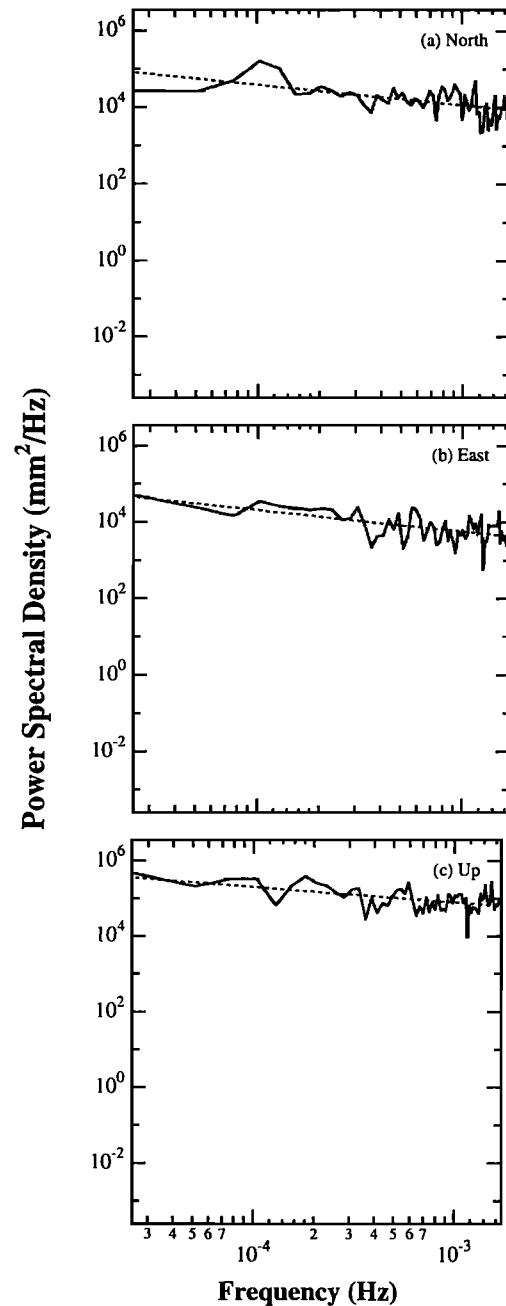


Figure 8. Same as Figures 5a–5c, except here for the time series shown in Figure 7. The estimated spectral indices are (a) -0.5 , (b) -0.6 , and (c) -0.4 .

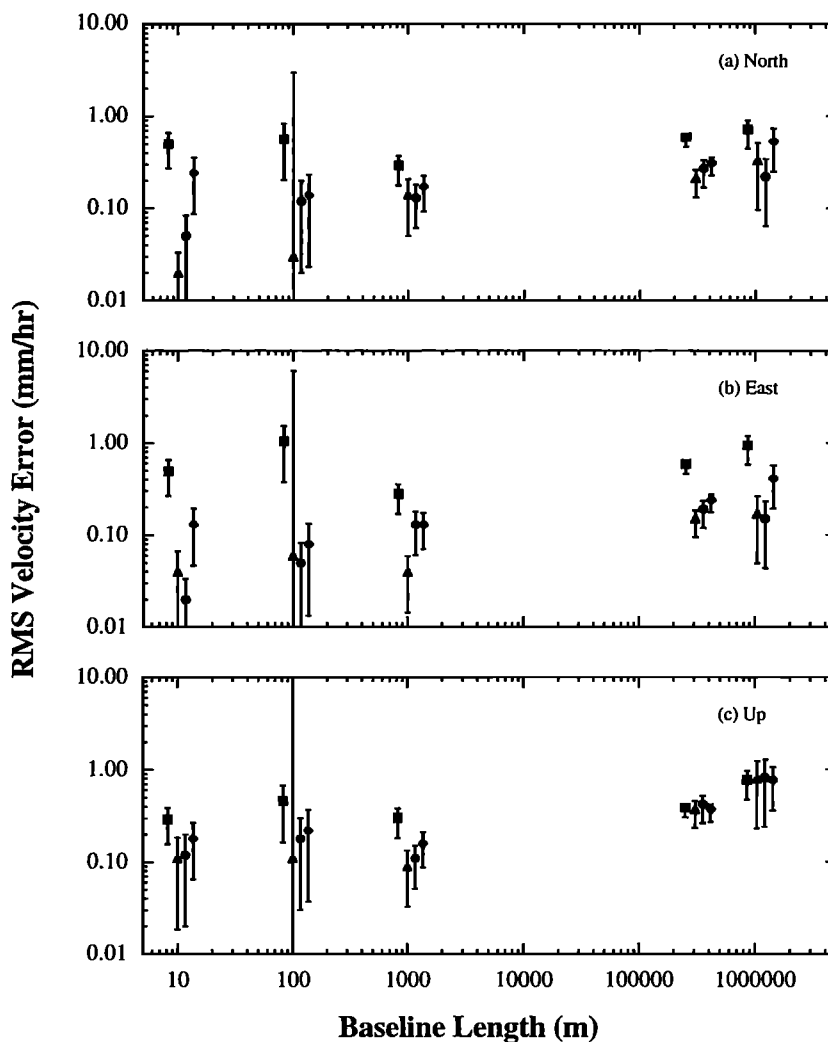


Figure 9. Root-mean-square (rms) velocity errors for different time spans used to determine the velocity of the three topocentric components: (a) north, (b) east, and (c) up. The rms velocity error for the ~ 300 -km baseline represents the average of the velocity errors of the eight baselines of similar length (lengths between 181.9 and 407.7 km; see Table 2). Error bars represent the 90% confidence interval. For each baseline length, the values for the different time spans have been shifted horizontally for clarity. Key to time spans: triangle, 24 hours; circle, 18 hours; diamond, 12 hours; and square, 6 hours.

estimates of velocity. To create the different time spans, the full ~ 30 -hour data set was binned with spans of 6, 12, 18, and 24 hours.

The rms errors for the rates for all baseline lengths, topocentric components, and time spans were found to be less than 1 mm h^{-1} . As we might expect, the errors generally increase with increasing baseline length or decreasing time span, and the errors for the vertical component are greater than those for the north component, which are greater than those for the east component. For all time spans but the 6-hour time span, the rms velocity errors for the horizontal components are less than 0.5 mm h^{-1} , and less than 0.3 mm h^{-1} for the 18- and 24-hour time spans. For the 24-hour time spans and 1000-m baseline, the rms velocity errors for the horizontal components are less than 0.15 mm h^{-1} .

The shortest distances in Figure 9 correspond to the ONSA to O-302 (10 m) and O-401 to O-302 (100 m) baselines. The baselines were formed, as discussed above (see also Table 1), by occupying the O-302 site with the moving platform. (Recall

from above that two blocks of data were lost at this site owing to receiver problems.) These shortest baseline points of Figure 9 therefore represent significantly fewer measurements than do the other points, and they are therefore less reliable. This decreased reliability is evident in the increased error bars for the rms velocity errors.

The component exhibiting the least variability in rms error as a function either of baseline length or time span is the vertical component. The minimum rms error observed for this component (24 hours, 10 m) is 0.1 mm h^{-1} , and the maximum (18 hours, 1044 km) is 0.9 mm h^{-1} , for a dynamic range of $\sim 10:1$. The dynamic range in rms error exhibited by the horizontal components is $\sim 50:1$. We can imagine several possible explanations for this difference, the most likely being that multipath and signal scattering, which can significantly affect the estimate of the vertical position (and hence presumably vertical velocity) are local effects, even near-field effects (in the case of signal scattering), which do not necessarily cancel even for very short baselines [Elósegui *et al.*, 1995].

Discussion and Conclusions

We have assumed in our analysis that the time-dependent position of the moving platform can be described by means of a suitable stochastic process. For this analysis, we have chosen to use a random walk model. This choice of stochastic process was based on the known motion of the antenna; the parallel between (1) and (2) indicated that modeling the position as a random walk is equivalent to modeling its velocity, the parameter of interest, as a white noise process. The random walk variability σ_{rw} can be related to the dynamic resolution parameter ξ_{rw} for an appropriate time interval Δt . Throughout this study, we have chosen $\xi_{rw} = 10$, which for $\Delta t = 300$ s gave us a value for σ_{rw} of $0.05 \text{ mm s}^{-1/2}$. The results presented in Figure 4 suggest that our choice for the value of σ_{rw} , based on the value of ξ_{rw} and Δt , represents nearly a lower limit for estimating unbiased velocities over a time span of 24 hours. From the same figure, the upper limit for the value of σ_{rw} corresponds to a value of $\xi_{rw} \approx 100$ for the same $\Delta t = 300$ s. An ideal "midrange" value for σ_{rw} can be obtained by either choosing $10 \leq \sigma_{rw} \leq 100$ for $\Delta t = 300$ s, as in Figure 4, or by choosing $300 \text{ s} \leq \Delta t \leq 8.3 \text{ hours}$ for $\xi_{rw} = 10$. We therefore conclude that to calculate a midrange input value for σ_{rw} for a given expected velocity, choose a value for $\xi_{rw} = 10$ and choose Δt to be a midrange value compared to the total time span.

We have found that using the random walk model significantly reduces the high-frequency noise in time-dependent estimates of site position. The spectral index obtained from power spectral density estimates of the position of the moving platform is about -4 and is controlled by the response of the Kalman filter. We found that the spectral index varies between $-4 \leq \alpha \leq -2$ as the dynamic resolution parameter ξ_{rw} varies between $10 \leq \xi_{rw} \leq 100$, and that $\alpha \leq -1$ for a white noise model. A white noise model might be more desirable than a random walk process under certain circumstances. For example, as noted by D. M. Tralli (submitted manuscript, 1995), a rapid offset such as might be associated with a seismic event is more properly modeled as a white noise process, whereas a random walk model would cause accommodation of the displacement by smoothing the estimated positions.

The sources of error in our determinations of velocity include near-field signal scattering and signal multipath, phase-center variations, atmospheric propagation, and satellite ephemerides. There may also be a small error associated with the changing near-field scattering environment as the table moves, although this effect will be small and possibly negligible, since the table moves horizontally a total of only 25.4 mm, and the area of the table is small in comparison with the aluminum plate (see section above, GPS Survey and Data Acquisition). This study, however, does not contain a detailed analysis of these sources of error. Signal scattering and signal multipath errors are caused by near-field and far-field signal reflection, respectively, from objects in the environment of the GPS antenna. These errors affect most significantly the estimates of the vertical component of site position, and are independent of baseline length [Elósegui *et al.*, 1995]. Two possible ways to reduce these errors are the use of microwave absorbing material around the antenna and the decrease of the gain of the GPS antenna for low elevation angles. We are currently studying these problems and will report our results in a future paper. Antenna phase-center variations are due to the nonsphericity of the antenna phase pattern. If the phase patterns of antennas of the same make and model are similar [Schupler *et al.*, 1994],

the short (≤ 1 km) baselines should be insensitive to this error. The phase-center variations of a Dorne-Margolin antenna with concentric choke rings amount to 10–14 mm, peak-to-peak, over an elevation range of 0° – 90° ; because the difference in elevation angle for antennas at the two ends of a ~ 1000 -km baseline for a given satellite at a given epoch is $\leq 10^\circ$, this error may affect mainly the estimates of the vertical component of the velocity for the longest baselines. Given the relatively short distances from the moving antenna to all the stationary antennas in our experiment, we expect the effect of satellite ephemeride errors on our results to be insignificant. The atmospheric propagation delays were not estimated in analyses involving short (≤ 1 km) baselines because their values for the two sites are nearly 100% correlated. It is possible that variations in the tropospheric path delay are the largest source of error in the results from analysis of our longest baselines. A thorough discussion of tropospheric path-delay errors on baselines longer than about 10 km and for timescales from a few minutes to over a day can be found in the work by D. M. Tralli (submitted manuscript, 1995).

In the near future, continuously recording GPS arrays will be used to study geophysical signals over short timescales on spatial scales of tens to hundreds of kilometers. The analysis presented here has clear implications for the use of GPS as a strain meter. The results presented in Figure 9 demonstrate that, for the detection of a constant velocity signal, GPS can achieve submillimeter-per-hour accuracy with subdaily-to-daily temporal resolution. For example, for strain measurements across a 10-m baseline with a sampling interval of 300 s, with an rms velocity error of 0.5 mm h^{-1} , as obtained for the north component, we could detect a strain rate of $50 \mu\epsilon \text{ h}^{-1}$ in a time span of 6 hours. Increasing the time span to 24 hours, an rms velocity error of 0.02 mm h^{-1} would provide a strain-rate standard error of $2 \mu\epsilon \text{ h}^{-1}$. A 1000-m baseline and identical sampling interval, with an rms velocity error of 0.2 mm h^{-1} , would yield a strain-rate error of $0.2 \mu\epsilon \text{ h}^{-1}$ in a time span of 6 hours. Over a similar baseline length (1000 m) sampled once per second, Genrich and Bock [1992] detected a strain of 1 – $2 \mu\epsilon$ in about 1 min with multipath modeling. The single-measurement error implied by this result would yield, over a time span of 6 hours with a sampling interval of 300 s, a velocity error of 0.5 – 1.0 mm h^{-1} . The velocity error that we obtained for this scale is comparable, although better by a factor about 2–3, possibly owing to the random walk model we used. For far-field strain measurements, for a ~ 1000 -km baseline with the same 300-s sampling interval, we obtained an rms velocity error of 0.7 mm h^{-1} , or a strain rate of $0.7 \text{ n}\epsilon \text{ h}^{-1}$ in a time span of 6 hours. Although baselines of the order of 10 km in length are missing in this study, one would expect that their rms velocity errors will be between the values for the 1000-m and 300-km baselines, and therefore fall in the range 0.2 – 0.6 mm h^{-1} , or equivalently, a strain-rate error of 20 – $60 \text{ n}\epsilon \text{ h}^{-1}$ within the time spans of interest. Over spatial scales of about 10 km, D. M. Tralli (submitted manuscript, 1995) obtained a short-term (subdaily) position error of 10–100 nm .

The intended application of this work is for the study of short-term ground motions in a geophysically dynamic environment. GPS can be used to reliably estimate 1 mm h^{-1} motions over a wide range of baseline lengths and time spans. Preseismic and postseismic motions, were they manifest at these magnitudes and timescales, could be estimated with permanent GPS networks at the 0.1 – 0.2 mm h^{-1} sensitivity level in a time span of 12 hours.

Acknowledgments. We would like to thank R. B. Langley for suggesting the use of a leadscrew system for translating the antenna. D. J. Oberlander and E. E. Bloemhof helped construct and calibrate the translation table. T. R. Carlsson assisted with the installation of the systems at Onsala Space Observatory. T. A. Herring, R. B. Langley, and the Associate Editor provided significant and useful comments. This work was supported by NASA grant NAG5-538, NSF grant EAR-9105502, and the Smithsonian Institution.

References

- Blewitt, G., Carrier phase ambiguity resolution for the Global Positioning System applied to geodetic baselines up to 2000 km, *J. Geophys. Res.*, *94*, 10,187–10,203, 1989.
- Blewitt, G., M. B. Heflin, K. J. Hurst, D. C. Jefferson, F. H. Webb, and J. F. Zumberge, Absolute far-field displacements from the 28 June 1992 Landers earthquake sequence, *Nature*, *361*, 340–342, 1993.
- Bock, Y., et al., Detection of crustal deformation from the Landers earthquake sequence using continuous geodetic measurements, *Nature*, *361*, 337–340, 1993.
- Boucher, C., Z. Altamimi, and L. Duhan (Eds.), Results and analysis of the ITRF93, *IERS Tech. Note 18*, Int. Earth Rotation Serv., Observ. de Paris, Paris, France, 1994.
- Davis, J. L., W. H. Prescott, J. L. Svarc, and K. Wendt, Assessment of Global Positioning System measurements for studies of crustal deformation, *J. Geophys. Res.*, *94*, 13,635–13,650, 1989.
- Davis, J. L., J. M. Johansson, I. I. Shapiro, J. X. Mitrovica, B. O. Rönnäng, G. Elgered, R. T. K. Jaldehag, M. Ekman, B. Jonsson, and G. Hedling, Geophysical applications of space geodetic measurements in Fennoscandia, in *Proceedings of the International Workshop for Reference Frame Establishment and Technical Development in Space Geodesy*, edited by J. Campbell, T. Yoshino, and T. Sasao, pp. 248–255, Science and Technology Agency of Japan, Tokyo, 1993.
- Dixon, T. H., An introduction to the Global Positioning System and some geological applications, *Rev. Geophys.*, *29*, 249–276, 1991.
- Dixon, T. H., GPS measurements of relative motion of the Cocos and Caribbean plates and strain accumulation across the Middle America Trench, *Geophys. Res. Lett.*, *20*, 2167–2170, 1993.
- Elósegui, P., J. L. Davis, R. T. K. Jaldehag, J. M. Johansson, A. E. Niell, and I. I. Shapiro, Geodesy using the Global Positioning System: The effects of signal scattering on estimates of site position, *J. Geophys. Res.*, *100*, 9921–9934, 1995.
- Feigl, K. L., et al., Space geodetic measurement of crustal deformation in central and southern California, *J. Geophys. Res.*, *98*, 21,617–21,712, 1993.
- Genrich, J. F., and Y. Bock, Rapid resolution of crustal motion at short ranges with the Global Positioning System, *J. Geophys. Res.*, *97*, 3261–3269, 1992.
- Hager, B. H., R. W. King, and M. H. Murray, Measurements of crustal deformation using the Global Positioning System, *Annu. Rev. Geophys.*, *19*, 351–382, 1991.
- Herring, T. A., J. L. Davis, and I. I. Shapiro, Geodesy by radio interferometry: The application of Kalman filtering to the analysis of very long baseline interferometry data, *J. Geophys. Res.*, *95*, 12,561–12,581, 1990.
- Hofmann-Wellenhof, B., H. Lichtenegger, and J. Collins, *GPS Theory and Practice*, 2nd ed., Springer-Verlag, New York, 1994.
- Johansson, J. M., R. T. K. Jaldehag, J. L. Davis, M. Ekman, G. Elgered, G. Hedling, J. X. Mitrovica, B. Jonsson, B. O. Rönnäng, and I. I. Shapiro, Scientific contributions of the Swedish IGS activities, in *Proceedings of the 1993 IGS Workshop*, edited by G. Beutler and E. Brockman, pp. 265–274, Druckerei der Universität Bern, Bern, Switzerland, 1993.
- King, R. W., E. G. Masters, C. Rizos, A. Stolz, and J. Collins, *Surveying With Global Positioning System*, 128 pp., Dümmler, Bonn, Germany, 1985.
- Lachapelle, G., GPS observables and error sources for kinematic positioning, in *Proceedings Kinematic Systems in Geodesy, Surveying, and Remote Sensing, IAG Symp. 107*, edited by K.-P. Schwarz and G. Lachapelle, pp. 17–26, Int. Assoc. of Geod., Copenhagen, 1990.
- Larson, K. M., Deformation in the southern California borderlands, *J. Geophys. Res.*, *98*, 21,713–21,726, 1993.
- Larson, K. M., and J. Freymuller, Relative motions of the Australian, Pacific, and Antarctic plates estimated by the Global Positioning System, *Geophys. Res. Lett.*, *22*, 37–40, 1995.
- Lichten, S. M., and J. S. Border, Strategies for high-precision Global Positioning System orbit determination, *J. Geophys. Res.*, *92*, 12,751–12,762, 1987.
- Liebelt, P. B., *An Introduction to Optimal Estimation*, Addison-Wesley, Reading, Mass., 1967.
- Press, W. H., B. P. Flannery, S. A. Teukolsky, and W. T. Vetterling, *Numerical Recipes in FORTRAN: The Art of Scientific Computing*, 963 pp., Cambridge Univ. Press, New York, 1992.
- Santerre, R., Impact of GPS satellite sky distribution, *Manuscr. Geod.*, *16*, 28–53, 1991.
- Schupler, B. R., R. L. Allshouse, and T. A. Clark, Signal characteristics of GPS user antennas, *Navigation*, *41*, 3277–3295, 1994.
- Schwarz, K. P., M. E. Cannon, and R. V. C. Wong, A comparison of GPS kinematic models for the determination of position and velocity along a trajectory, *Manuscr. Geod.*, *14*, 345–353, 1989.
- Shen, Z.-K., D. D. Jackson, Y. Feng, M. Cline, M. Kim, P. Fang, and Y. Bock, Postseismic deformation following the Landers earthquake, California, 28 June 1992, *Bull. Seismol. Soc. Am.*, *84*, 780–791, 1994.
- Shimada, S., and Y. Bock, Crustal deformation in central Japan determined by a Global Positioning System fixed-point network, *J. Geophys. Res.*, *97*, 12,437–12,455, 1992.
- Tatarskii, V. I., *Wave Propagation in a Turbulent Medium*, translated from Russian by R. A. Silverman, McGraw-Hill, New York, 1961.
- Webb, F. H., and J. F. Zumberge, An introduction to the GIPSY/OASIS-II, *JPL Publ.*, *D-11088*, 1993.
- Webb, F. H., M. Bursik, T. Dixon, F. Farina, G. Marshall, and R. S. Stein, Inflation of Long Valley caldera from one year of continuous GPS observations, *Geophys. Res. Lett.*, *22*, 195–198, 1995.
- Wei, M., S. Ferguson, and K. P. Schwarz, Accuracy of GPS-derived acceleration from moving platform tests, in *From Mars to Greenland: Charting Gravity With Space and Airborne Instruments: Fields, Tides, Methods, Results, Proc. IAG Symp. 110*, edited by O. L. Colombo, pp. 235–249, Int. Assoc. of Geod., Copenhagen, 1991.
- Zumberge, J. F., D. C. Jefferson, M. B. Heflin, and F. H. Webb, Earth orientation results from the Jet Propulsion Laboratory using GPS, in *Earth Orientation, Reference Frames and Atmospheric Excitation Functions Submitted for the 1993 IERS Annual Report, IERS Tech. Note 17*, edited by P. Charlot, pp. P43–P47, Int. Earth Rotation Serv., Observ. de Paris, Paris, France, 1994.

J. L. Davis, P. Elósegui, and I. I. Shapiro, Harvard-Smithsonian Center for Astrophysics, 60 Garden Street, MS 42, Cambridge, MA 02138. (e-mail: jdavis@cfa.harvard.edu)
J. M. Johansson, Onsala Space Observatory, Chalmers University of Technology, S-439 92 Onsala, Sweden.

(Received May 2, 1995; revised November 15, 1995; accepted January 25, 1996.)